

# Wave propagation in a fractional viscoelastic Andrade medium: diffusive approximation and numerical modeling

A. Ben Jazia<sup>a</sup>, B. Lombard<sup>b,\*</sup>, C. Bellis<sup>b</sup>.

<sup>a</sup>*Ecole Centrale Marseille, 13451 Marseille, France*

<sup>b</sup>*LMA, CNRS, UPR 7051, Aix-Marseille Univ., Centrale Marseille, F-13402 Marseille Cedex 20, France*

---

## Abstract

This study focuses on the numerical modeling of wave propagation in fractionally-dissipative media. These viscoelastic models are such that the attenuation is frequency dependent and follows a power law with non-integer exponent. As a prototypical example, the Andrade model is chosen for its simplicity and its satisfactory fits of experimental flow laws in rocks and metals. The corresponding constitutive equation features a fractional derivative in time, a non-local term that can be expressed as a convolution product which direct implementation bears substantial memory cost. To circumvent this limitation, a diffusive representation approach is deployed, replacing the convolution product by an integral of a function satisfying a local time-domain ordinary differential equation. An associated quadrature formula yields a local-in-time system of partial differential equations, which is then proven to be well-posed. The properties of the resulting model are also compared to those of the original Andrade model. The quadrature scheme associated with the diffusive approximation, and constructed either from a classical polynomial approach or from a constrained optimization method, is investigated to finally highlight the benefits of using the latter approach. Wave propagation simulations in homogeneous domains are performed within a split formulation framework that yields an optimal stability condition and which features a joint fourth-order time-marching scheme coupled with an exact integration step.

---

\*Corresponding author

*Email addresses:* `abderrahim.ben-jazia@centrale-marseille.fr` (A. Ben Jazia), `lombard@lma.cnrs-mrs.fr` (B. Lombard), `bellis@lma.cnrs-mrs.fr` (C. Bellis)

A set of numerical experiments is presented to assess the efficiency of the diffusive approximation method for such wave propagation problems.

*Keywords:* Viscoelasticity; Andrade model; Fractional derivatives; Transient wave propagation; Finite differences

---

## 1. Introduction

There is a long history of studies discussing or providing experimental evidences of frequency-dependent viscoelastic attenuations, as observed in e.g. metals [1], acoustic media [2, 3] and in the Earth [4, 5]. Such a behavior is classically modeled using a fractional derivative operator [6, 7], a mathematical tool generalizing to real parameters the standard derivatives of integer orders [8]. While fractional calculus is now a mature theory in the field of viscoelasticity [9], some issues remain commonly encountered. They mostly revolve around the two questions of: (1) incorporating fractional dissipation into viscoelastic models that both fit experimental data and have a theoretical validity regarding, e.g., causality properties [10, 11] or the Kramers-Kronig relations [12]; and (2) implementing numerically these fractional models to perform wave propagation simulations. The latter problem is commonly tackled using standard approaches [13] for modeling constant-law of attenuation over a frequency-band of interest, i.e. with the fractional viscoelastic model being approximated by multiple relaxation mechanisms [14].

Bearing in mind the issue (1) discussed above, it is chosen to anchor the present study to a specific, yet prototypical, physically-based viscoelastic model, namely the Andrade model. Initially introduced in [1] to fit experimental flow laws in metals, it has been further investigated in [15]. It is now used as a reference in a number of studies [16, 17, 18, 19] for the description of observed frequency-dependent damping behaviors in the field of geophysics and experimental rock mechanics. Moreover, the Andrade model creep function, as written, can notably be decomposed into a fractional power-law added to a standard Maxwell viscoelastic model. Therefore, while being physically motivated and rooted in experiments, this model gives leeway to cover the spectrum from a conventional rheologi-

24 cal mechanism to a more complex fractional model, and this with only a few parameters.

25

26 This study focuses on the issue (2), namely the numerical modeling of wave propa-  
27 gation within a fractionally-dissipative Andrade medium. The objective is to develop an  
28 efficient approximation strategy of the fractional term featured in this viscoelastic model in  
29 view of the investigation and simulation of its transient dynamical behavior. A model-based  
30 approximation approach is explored in the sense that the original constitutive equation is  
31 not intended to be superseded by another viscoelastic model, *per se*, which would be de-  
32 signed to fit only a given observable, such as the quality factor, or overall behavior.

33

34 The article aim and contribution are twofold:

35 (i) Deploy an approximation of the fractional derivative featured in the constitutive  
36 equation considered. A direct discretization of this term, that is associated with a non-local  
37 time-domain convolution product [8] requires the storage of the entire variables history.  
38 While being potentially improved by Grünwald-Letnikov finite-difference approximation  
39 schemes, see e.g. [20], such an approach remains costly numerically and is therefore cir-  
40 cumvented. Alternatively, a so-called diffusive representation is preferred [21], as it allows  
41 to recast the equations considered into a local-in-time system while introducing only a lim-  
42 ited number of additional memory variables in its discretized form [22]. Following later  
43 improvements of the method in [23, 24, 25, 26], an efficient quadrature scheme is investi-  
44 gated in order to obtain a satisfactory fit of the reference model compliance.

45 (ii) Implement the resulting approximated model into a wave propagation scheme.  
46 While the available literature on the numerical simulation of transient wave propagation  
47 within fractionally-damped media is relatively scarce, see e.g. [27, 28], the aim is here to  
48 demonstrate the practicality and efficiency of the proposed approach. For the sake of sim-  
49 plicity, the viscoelastic medium considered is assumed to be unidimensional and homoge-  
50 neous. After discretization of the dynamical system at hand, a Strang splitting approach  
51 [29] is adopted, both to reach an optimal stability condition and to enable the use of an effi-

52 cient high-order time-marching scheme coupled with an exact integration step. Moreover,  
 53 deriving a semi-analytical solution for the configuration considered, as a baseline, a set  
 54 of numerical results is presented to assess the quality of the numerical scheme developed.  
 55 The overall features and performances of the diffusive representation are finally discussed  
 56 to compare the original Andrade model with its diffusive approximated counterpart.

57

58 This article is organized as follows. The reference Andrade model is presented and  
 59 discussed in Section 2. Considering the featured fractional derivative, a corresponding  
 60 diffusive approximated version of the former is subsequently formulated and referred to  
 61 as the Andrade–DA model. The evolution problem is investigated in Section 3, with the  
 62 derivation and analysis of the first-order hyperbolic system associated with the Andrade–  
 63 DA model. Section 4.1 is concerned with the definition and computation of an efficient  
 64 quadrature scheme for the diffusive approximation, while the implementation of the fully  
 65 discretized system is described in Section 4.2. Corresponding numerical results are pre-  
 66 sented and discussed in Section 5.

## 67 2. Fractional viscoelastic model

### 68 2.1. Preliminaries

69 The causal constitutive law describing the behavior of a 1D linear viscoelastic medium  
 70 can be expressed in terms of the time-domain convolution

$$\varepsilon(t) = \int_0^t \chi(t - \tau) \frac{\partial \sigma}{\partial \tau}(\tau) \, d\tau, \quad (1)$$

71 with creep function  $\chi$ , stress field  $\sigma$  and strain field  $\varepsilon = \partial u / \partial x$  associated with unidimen-  
 72 sional displacement  $u$ .

73 Next, for parameters satisfying  $0 < \beta < 1$ , the so-called Caputo-type fractional deriva-  
 74 tive [7, 9, 8] of a causal function  $g(t)$  is defined as

$$\frac{d^\beta g}{dt^\beta}(t) = \frac{1}{\Gamma(1 - \beta)} \int_0^t (t - \tau)^{-\beta} \frac{dg}{d\tau}(\tau) \, d\tau, \quad (2)$$

75 where  $\Gamma$  is the Gamma function. Defining the direct and inverse Fourier transforms in time  
 76 of a function  $g(t)$  as

$$\hat{g}(\omega) = \int_{-\infty}^{+\infty} g(t)e^{-i\omega t} dt, \quad g(t) = \frac{1}{2\pi} \int_{-\infty}^{+\infty} \hat{g}(\omega)e^{i\omega t} d\omega,$$

77 then the frequency-domain counterpart of equation (2) reads

$$\widehat{\left[\frac{d^\beta g}{dt^\beta}\right]}(\omega) = (i\omega)^\beta \hat{g}(\omega), \quad (3)$$

78 so that definition (2) is a straightforward generalization of the derivative of integer order.

## 79 2.2. Andrade model

80 The Andrade model [1] is characterized by the creep function given by

$$\chi(t) = \left[ J_u + \frac{t}{\eta} + A t^\alpha \right] H(t), \quad 0 < \alpha < 1, \quad (4)$$

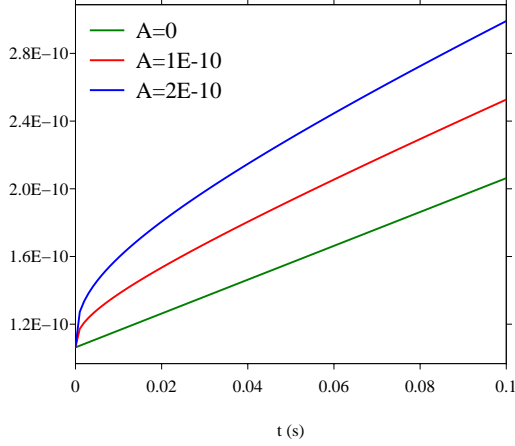
81 with Heaviside step function  $H(t)$ , unrelaxed compliance  $J_u$ , viscosity  $\eta$  and two positive  
 82 physical parameters  $A$  and  $\alpha$ . Usual fits with experimental data correspond to  $\frac{1}{3} \leq \alpha \leq \frac{1}{2}$   
 83 [15, 16]. The composite law (4) can be additively decomposed into a standard Maxwell  
 84 rheological mechanism with creep function  $t \mapsto J_u + t/\eta$  and a relaxation time  $\tau_{\text{Mx}} = \eta J_u$ ,  
 85 together with a power law dependence in time  $t \mapsto A t^\alpha$  which constitutes its main feature.  
 86 Examples behaviors of the creep function (4) are illustrated in Figure 1a.

87 The frequency-domain compliance  $N = i\omega\hat{\chi}$ , and such that  $\hat{\varepsilon} = N \hat{\sigma}$  according to the  
 88 Fourier transform of equation (1), can be deduced from (4) as

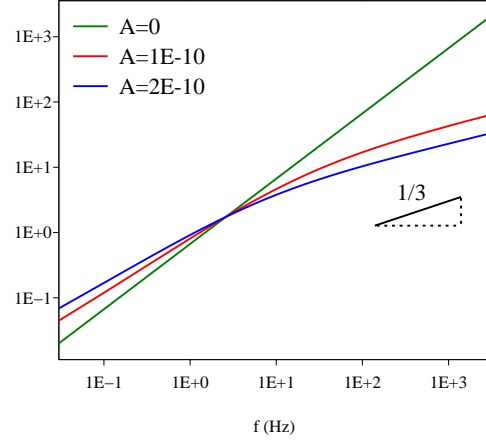
$$N(\omega) = J_u - \frac{i}{\eta\omega} + A\Gamma(1 + \alpha)(i\omega)^{-\alpha}. \quad (5)$$

89 Straightforward manipulations on (3), (4) and (5) lead to the following constitutive equa-  
 90 tion in differential form for the Andrade model

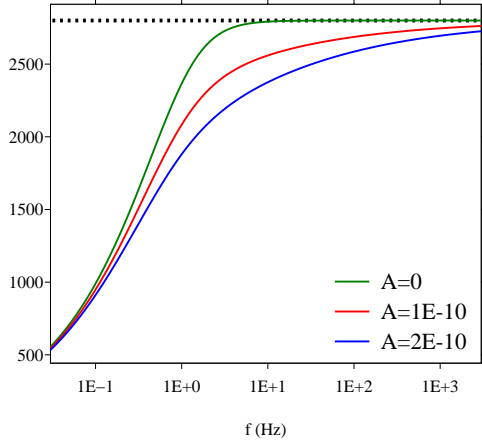
$$\frac{\partial \varepsilon}{\partial t} = J_u \frac{\partial \sigma}{\partial t} + \frac{1}{\eta} \sigma + A\Gamma(1 + \alpha) \frac{\partial^{1-\alpha}}{\partial t^{1-\alpha}} \sigma. \quad (6)$$



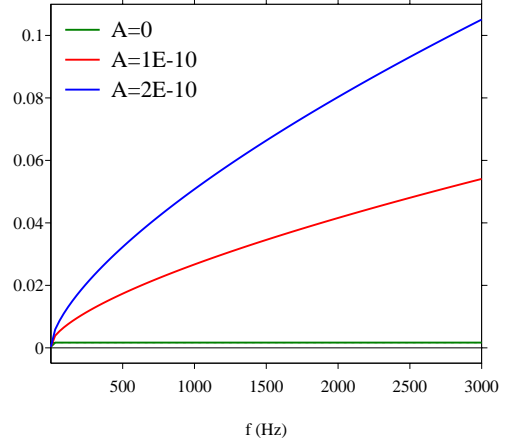
(a) Creep function  $\chi(t)$



(b) Quality factor  $Q(f)$



(c) Phase velocity  $c(f)$



(d) Attenuation  $\zeta(f)$

Figure 1: Behaviors of various viscoelastic models derived from (4): Maxwell model ( $A = 0$ ) and Andrade model ( $\alpha = 1/3$ , with  $A = 10^{-10} \text{ Pa}^{-1} \cdot \text{s}^{-\alpha}$  and  $A = 2.10^{-10} \text{ Pa}^{-1} \cdot \text{s}^{-\alpha}$ ). The other physical parameters are:  $\rho = 1200 \text{ kg/m}^3$ ,  $c_\infty = 2800 \text{ m/s}$  and  $\eta = 10^9 \text{ Pa} \cdot \text{s}$ . The horizontal dotted line in panel (c) denotes the high-frequency limit  $c_\infty$ .

91 **2.3. Dispersion relations**

92 The complex wave number  $k(\omega)$  satisfies

$$k(\omega) = \sqrt{\rho} \omega [N(\omega)]^{1/2} := \frac{\omega}{c(\omega)} - i\zeta(\omega), \quad (7)$$

93 where the phase velocity  $c$  and the attenuation  $\zeta$  are given by

$$c(\omega) = \sqrt{\frac{2}{\rho(|N| + \operatorname{Re}[N])}}, \quad \zeta(\omega) = \omega \sqrt{\frac{\rho(|N| - \operatorname{Re}[N])}{2}}. \quad (8)$$

94 Owing to equations (5) and (8), the following limits hold:

$$\begin{aligned} \lim_{\omega \rightarrow 0} c(\omega) &= 0, & \lim_{\omega \rightarrow +\infty} c(\omega) &= \frac{1}{\sqrt{\rho J_u}} := c_\infty, \\ \lim_{\omega \rightarrow 0} \zeta(\omega) &= 0, & \lim_{\omega \rightarrow +\infty} \zeta(\omega) &= +\infty. \end{aligned} \quad (9)$$

95 Moreover, when  $A > 0$ , the creep function (4) is an increasing and concave function.

96 As a consequence, owing to the theoretical developments in [30] and [31], the attenuation

97  $\zeta(\omega)$  for the Andrade model turns out to be sublinear in the high-frequency range, i.e.

$$\zeta(\omega) \underset{\omega \rightarrow +\infty}{=} o(\omega). \quad (10)$$

98 This key property confirms the relevance of the choice of the Andrade model as a proto-  
99 typical example of fractional viscoelastic media.

100 The quality factor  $Q$  is defined as the ratio

$$Q(\omega) = -\frac{\operatorname{Re}[k^2]}{\operatorname{Im}[k^2]} = -\frac{\operatorname{Re}[N]}{\operatorname{Im}[N]}. \quad (11)$$

101 According to (5) and in a high-frequency regime, the frequency-dependent behavior fol-  
102 lows

$$Q(\omega) \underset{\omega \rightarrow +\infty}{\sim} Q_\infty \omega^\alpha \quad \text{with } Q_\infty = J_u \left[ A \Gamma(1 + \alpha) \sin\left(\frac{\alpha\pi}{2}\right) \right]^{-1}. \quad (12)$$

103 Sample behaviors of the Andrade model for  $\alpha = 1/3$  and a varying parameter  $A$  are  
104 sketched in Figure 1. Notably, the case  $A = 0$  corresponds to the standard Maxwell model.

105 When  $A \neq 0$ , one observes in Fig. 1b the slope  $1/3$  of the quality factor in log-log scale  
106 at high frequencies, as expected from (12). The attenuation  $\zeta$  is represented as a function

107 of the frequency  $f$  and displayed in linear scale in Fig. 1d to emphasize the sublinear  
108 high-frequency behavior (10).

109 2.4. Diffusive approximation: Andrade–DA model

110 When implementing (6), the difficulty revolves around the computation of the con-  
 111 volution product in (2) associated with the fractional derivative of order  $1 - \alpha$ , which is  
 112 numerically memory-consuming. The alternative approach adopted in this study is based  
 113 on a diffusive representation, and its approximation, of fractional derivatives. Following  
 114 [23], then for  $0 < \alpha < 1$  equation (2) can be recast as

$$\frac{\partial^{1-\alpha}}{\partial t^{1-\alpha}} \sigma = \int_0^{+\infty} \phi(x, t, \theta) \, d\theta, \quad (13)$$

115 where the function  $\phi$  is defined owing to a change of variables as

$$\phi(x, t, \theta) = \frac{2 \sin(\pi\alpha)}{\pi} \theta^{1-2\alpha} \int_0^t \frac{\partial \sigma}{\partial \tau}(x, \tau) e^{-(t-\tau)\theta^2} \, d\tau. \quad (14)$$

116 As  $\phi$  is expressed in terms of an integral operator with decaying exponential kernel, it  
 117 is referred to as a *diffusive* variable. From equation (14), it can be shown to satisfy the  
 118 following first-order differential equation for  $\theta > 0$ :

$$\begin{cases} \frac{\partial \phi}{\partial t} = -\theta^2 \phi + \frac{2 \sin(\pi\alpha)}{\pi} \theta^{1-2\alpha} \frac{\partial \sigma}{\partial t}, \\ \phi(x, 0, \theta) = 0. \end{cases} \quad (15)$$

119 The diffusive representation (13–14) amounts to supersede the non-local term in (6) by an  
 120 integral of the function  $\phi(x, t, \cdot)$  obeying the local first-order ordinary differential equa-  
 121 tion (15). The integral featured in (13) is in turn well-suited to be approximated using a  
 122 quadrature scheme, so that

$$\frac{\partial^{1-\alpha}}{\partial t^{1-\alpha}} \sigma \simeq \sum_{\ell=1}^L \mu_\ell \phi(x, t, \theta_\ell) \equiv \sum_{\ell=1}^L \mu_\ell \phi_\ell(x, t), \quad (16)$$

123 given a number  $L$  of quadrature nodes  $\theta_\ell$  with associated weights  $\mu_\ell$ , whose computations  
 124 will be returned to in Section 4.1.

125

126 The frequency-domain versions of equations (6), (15) and (16) lead to the approximated  
 127 complex compliance  $\tilde{N}$ , such that  $\hat{\varepsilon} = \tilde{N} \hat{\sigma}$  and characterizing the model hereafter referred



128 to as the Andrade–DA model, as

$$\tilde{N}(\omega) = J_u - \frac{i}{\eta\omega} + A\Gamma(1 + \alpha) \frac{2 \sin(\pi\alpha)}{\pi} \sum_{\ell=1}^L \mu_\ell \frac{\theta_\ell^{1-2\alpha}}{\theta_\ell^2 + i\omega}. \quad (17)$$

129 The diffusive approximated counterparts of (7) and (8) can be immediately deduced from  
 130 (17). In particular, the low-frequency and high-frequency limits of the phase velocity  $\tilde{c}$   
 131 are equal to those in (9). Moreover, using tables of standard Fourier transforms, the corre-  
 132 sponding time-domain creep function  $\tilde{\chi}$ , defined by  $\tilde{N} = i\omega\hat{\chi}$ , is obtained as

$$\tilde{\chi}(t) = \left[ J_u + \frac{t}{\eta} + A\Gamma(1 + \alpha) \frac{2 \sin(\pi\alpha)}{\pi} \sum_{\ell=1}^L \mu_\ell \theta_\ell^{-1-2\alpha} \left( 1 - e^{-\theta_\ell^2 t} \right) \right] H(t). \quad (18)$$

### 133 3. Evolution equations

134 With the complex compliance (17) of the Andrade–DA model at hand, which con-  
 135 stitutes the approximated version of the diffusive representation of the original Andrade  
 136 model (5), the present section is concerned with the description and analysis of its dynam-  
 137 ical behavior.

#### 138 3.1. First-order system

139 Let define the parameters

$$\gamma_{\ell,\alpha} = \frac{2 \sin(\pi\alpha)}{\pi J_u} \theta_\ell^{1-2\alpha}, \quad \Upsilon_{\ell,\alpha} = A\Gamma(1 + \alpha) \gamma_{\ell,\alpha} \quad \text{for } \ell = 1, \dots, L. \quad (19)$$

Combining the conservation of momentum in terms of velocity field  $v = \partial u / \partial t$  and equa-  
 tions (6), (15) and (16) yields

$$\left\{ \begin{array}{l} \frac{\partial v}{\partial t} - \frac{1}{\rho} \frac{\partial \sigma}{\partial x} = F_v, \end{array} \right. \quad (20a)$$

$$\left\{ \begin{array}{l} \frac{\partial \sigma}{\partial t} - \frac{1}{J_u} \frac{\partial v}{\partial x} = -\frac{1}{J_u \eta} \sigma - \frac{A\Gamma(1 + \alpha)}{J_u} \sum_{j=1}^L \mu_j \phi_j + F_\sigma, \end{array} \right. \quad (20b)$$

$$\left\{ \begin{array}{l} \frac{\partial \phi_\ell}{\partial t} - \gamma_{\ell,\alpha} \frac{\partial v}{\partial x} = -\theta_\ell^2 \phi_\ell - \frac{\gamma_{\ell,\alpha}}{\eta} \sigma - \Upsilon_{\ell,\alpha} \sum_{j=1}^L \mu_j \phi_j + J_u \gamma_{\ell,\alpha} F_\sigma, \end{array} \right. \quad (20c)$$

140 for  $\ell = 1, \dots, L$  and where  $F_v$  and  $F_\sigma$  are introduced to model external sources. Equations  
 141 (20) are completed by initial conditions

$$v(x, 0) = 0, \quad \sigma(x, 0) = 0, \quad \phi_\ell(x, 0) = 0 \quad \text{for } \ell = 1, \dots, L.$$

142 Gathering unknown and sources terms, let the vectors  $\mathbf{U}$  and  $\mathbf{F}$  be defined as

$$\mathbf{U} = [v, \sigma, \phi_1, \dots, \phi_L]^\top, \quad \mathbf{F} = [F_v, F_\sigma, J_u \gamma_{1,\alpha} F_\sigma, \dots, J_u \gamma_{L,\alpha} F_\sigma]^\top. \quad (21)$$

143 Then the system (20) can be written in the matrix-form

$$\frac{\partial \mathbf{U}}{\partial t} + \mathbf{A} \frac{\partial \mathbf{U}}{\partial x} = \mathbf{S} \mathbf{U} + \mathbf{F}, \quad (22)$$

144 where  $\mathbf{A}$  is given by

$$\mathbf{A} = \begin{bmatrix} 0 & -\rho^{-1} & 0 & \dots & 0 \\ -J_u^{-1} & 0 & 0 & \dots & 0 \\ -\gamma_{1,\alpha} & 0 & 0 & \dots & 0 \\ \vdots & \vdots & \vdots & \ddots & \vdots \\ -\gamma_{L,\alpha} & 0 & 0 & \dots & 0 \end{bmatrix}, \quad (23)$$

145 and  $\mathbf{S}$  reads

$$\mathbf{S} = \begin{bmatrix} 0 & 0 & 0 & \dots & 0 \\ 0 & -(J_u \eta)^{-1} & -A\Gamma(1 + \alpha) J_u^{-1} \mu_1 & \dots & -A\Gamma(1 + \alpha) J_u^{-1} \mu_L \\ 0 & -\gamma_{1,\alpha} \eta^{-1} & -\theta_1^2 - \Upsilon_{1,\alpha} \mu_1 & \dots & -\Upsilon_{1,\alpha} \mu_L \\ \vdots & \vdots & \vdots & \ddots & \vdots \\ 0 & -\gamma_{L,\alpha} \eta^{-1} & -\Upsilon_{L,\alpha} \mu_1 & \dots & -\theta_L^2 - \Upsilon_{L,\alpha} \mu_L \end{bmatrix}. \quad (24)$$

146 Note that this differential system remains valid in the case of a *non-homogeneous* vis-  
 147 coelastic medium.

### 148 3.2. Energy decay

149 Studying the energy associated with the system (20) is required to characterize the sta-  
 150 bility of the Andrade–DA model and to provide constraints on the diffusive approximation

151 calculation. For an infinite 1D domain, the stored kinetic and elastic energies are defined  
 152 as

$$\mathcal{E}_v(t) = \frac{1}{2} \int_{-\infty}^{+\infty} \rho v^2 dx \quad \text{and} \quad \mathcal{E}_\sigma(t) = \frac{1}{2} \int_{-\infty}^{+\infty} J_u \sigma^2 dx,$$

153 together with a coupled term associated with the diffusive approximation

$$\mathcal{E}_d(t) = \frac{1}{2} \int_{-\infty}^{+\infty} \sum_{\ell=1}^L \frac{\mu_\ell \Upsilon_{\ell,\alpha}}{\theta_\ell^2} \left( \sqrt{J_u} \sigma - \frac{\phi_\ell}{\sqrt{J_u} \gamma_{\ell,\alpha}} \right)^2 dx.$$

154 Then, in the absence of any source term, one has the following property

155 **Proposition 1.** *If  $\mu_\ell > 0$  for all  $\ell = 1, \dots, L$ , then the function  $\mathcal{E}(t) = \mathcal{E}_v(t) + \mathcal{E}_\sigma(t) + \mathcal{E}_d(t)$   
 156 is a positive definite quadratic form and  $\frac{d\mathcal{E}}{dt} < 0$  for all time  $t > 0$ .*

157 *Proof.* In the absence of any source term, then multiplying the momentum equation (20a)  
 158 by the velocity field  $v$  and integrating spatially by part yields

$$\int_{-\infty}^{+\infty} \left\{ \rho v \frac{\partial v}{\partial t} + \sigma \frac{\partial v}{\partial x} \right\} dx = 0,$$

159 assuming that the elastic fields vanish at infinity. Likewise, from equation (20b) and mul-  
 160 tiplying by  $\sigma$ , one obtains

$$\frac{1}{2} \frac{d}{dt} \int_{-\infty}^{+\infty} \{ \rho v^2 + J_u \sigma^2 \} dx + \int_{-\infty}^{+\infty} \left\{ \frac{\sigma^2}{\eta} + A\Gamma(1+\alpha) \sum_{\ell=1}^L \mu_\ell \phi_\ell \sigma \right\} dx = 0. \quad (25)$$

161 Now, using twice differential equation (15), one has for  $\ell = 1, \dots, L$

$$\sigma \frac{\partial \phi_\ell}{\partial t} + \theta_\ell^2 \phi_\ell \sigma - J_u \gamma_{\ell,\alpha} \sigma \frac{\partial \sigma}{\partial t} = 0 \quad \text{and} \quad \frac{\phi_\ell}{J_u \gamma_{\ell,\alpha}} \frac{\partial \phi_\ell}{\partial t} + \frac{\theta_\ell^2 \phi_\ell^2}{J_u \gamma_{\ell,\alpha}} - \phi_\ell \frac{\partial \sigma}{\partial t} = 0,$$

162 which after subtraction and manipulation entails

$$\phi_\ell \sigma = \frac{\phi_\ell^2}{J_u \gamma_{\ell,\alpha}} + \frac{\gamma_{\ell,\alpha}}{2\theta_\ell^2} \frac{d}{dt} \left( \sqrt{J_u} \sigma - \frac{\phi_\ell}{\sqrt{J_u} \gamma_{\ell,\alpha}} \right)^2. \quad (26)$$

Finally, substituting (26) in (25) leads to the relation

$$\begin{aligned} \frac{1}{2} \frac{d}{dt} \int_{-\infty}^{+\infty} \left\{ \rho v^2 + J_u \sigma^2 + \sum_{\ell=1}^L \frac{\mu_\ell \Upsilon_{\ell,\alpha}}{\theta_\ell^2} \left( \sqrt{J_u} \sigma - \frac{\phi_\ell}{\sqrt{J_u} \gamma_{\ell,\alpha}} \right)^2 \right\} dx \\ = - \int_{-\infty}^{+\infty} \left\{ \frac{\sigma^2}{\eta} + \sum_{\ell=1}^L \mu_\ell \Upsilon_{\ell,\alpha} \left( \frac{\phi_\ell}{\sqrt{J_u} \gamma_{\ell,\alpha}} \right)^2 \right\} dx, \end{aligned}$$

163 which concludes the proof.  $\square$

164 In summary, positivity of the quadrature nodes and weights in (16) is crucial to ensure  
 165 the well-posedness of the system (20). This issue will be further discussed in Section 4.1.

### 166 3.3. Properties of matrices

167 Some properties of the matrices  $\mathbf{A}$  (23) and  $\mathbf{S}$  (24) are discussed to characterize the  
 168 first-order system (22) of partial differential equations.

169 **Proposition 2.** *The eigenvalues of the matrix  $\mathbf{A}$  are*

$$\text{sp}(\mathbf{A}) = \{0, \pm c_\infty\}, \quad \text{with } 0 \text{ being of multiplicity } L.$$

170 As  $\mathbf{A}$  is diagonalizable with real eigenvalues, then equation (22) is a hyperbolic system  
 171 of partial differential equations, with solutions of finite-velocity. It is emphasized that the  
 172 eigenvalue  $c_\infty = 1/\sqrt{\rho J_u}$  does not depend on the quadrature coefficients  $\{(\mu_\ell, \theta_\ell)\}_\ell$ , so  
 173 that the phase velocity upper bounds for the Andrade and Andrade–DA models are equal.

174 **Proposition 3.** *Assuming  $\theta_\ell > 0$  and  $\mu_\ell > 0$  for  $\ell = 1, \dots, L$  then  $\text{sp}(\mathbf{S}) \ni 0$  with  
 175 multiplicity 1. Moreover the  $L + 1$  non-zero eigenvalues  $\lambda_\ell$  of  $\mathbf{S}$  are real and, ordering the  
 176 nodes as  $0 < \theta_1 < \dots < \theta_L$ , satisfy*

$$\lambda_{L+1} < -\theta_L^2 < \dots < -\theta_\ell^2 < \lambda_\ell < -\theta_{\ell-1}^2 < \dots < \lambda_1 < 0.$$

177

178 *Proof.* Let  $\mathcal{P}_S(\lambda)$  denote the characteristic polynomial of the matrix  $\mathbf{S}$ , i.e.  $\mathcal{P}_S(\lambda) =$   
 179  $\det(\mathbf{S} - \lambda \mathbf{I}_{L+2})$  with  $\mathbf{I}_{L+2}$  the  $(L + 2)$ -identity matrix. The line  $i$  and the column  $j$  of  
 180 the determinant are denoted by  $\mathcal{L}_i$  and  $\mathcal{C}_j$ , respectively. The following algebraic manipula-  
 181 tions are performed successively:

182 (i)  $\mathcal{L}_j \leftarrow \mathcal{L}_j - \gamma_\alpha \theta_j^{1-2\alpha} \mathcal{L}_1$  with  $j = 2, \dots, L + 1$

183 (ii)  $\mathcal{C}_1 \leftarrow \mathcal{C}_1 \prod_{\ell=1}^L (-\theta_\ell^2 - \lambda)$

184 (iii)  $\mathcal{C}_1 \leftarrow \mathcal{C}_1 - \gamma_\alpha \theta_\ell^{1-2\alpha} \lambda \mathcal{C}_\ell \prod_{\substack{i=1 \\ i \neq \ell}}^L (-\theta_i^2 - \lambda)$  for  $\ell = 2, \dots, L + 1$ .

185 From (24) and definition (19) of parameters  $\gamma_{\ell,\alpha}$  and  $\Upsilon_{\ell,\alpha}$ , one deduces

$$\mathcal{P}_{\mathbf{S}}(\lambda) = \lambda \left[ \left( (J_u \eta)^{-1} + \lambda \right) \prod_{\ell=1}^L (-\theta_{\ell}^2 - \lambda) + \lambda \sum_{\ell=1}^L \mu_{\ell} \Upsilon_{\ell,\alpha} \prod_{\substack{j=1 \\ j \neq \ell}}^L (-\theta_j^2 - \lambda) \right] := \lambda \mathcal{Q}_{\mathbf{S}}(\lambda).$$

186 From the above equation, one has  $\mathcal{P}_{\mathbf{S}}(0) \neq 0$  while  $\mathcal{Q}_{\mathbf{S}}(0) \neq 0$ , therefore 0 is an eigenvalue  
187 of the matrix  $\mathbf{S}$  with multiplicity 1. In the limit  $\lambda \rightarrow 0$ , then asymptotically

$$\mathcal{P}_{\mathbf{S}}(\lambda) \underset{\lambda \rightarrow 0}{\sim} (-1)^L (J_u \eta)^{-1} \lambda \prod_{\ell=1}^L \theta_{\ell}^2, \quad \text{so that} \quad \text{sgn}(\mathcal{P}_{\mathbf{S}}(0^-)) = (-1)^{L+1}. \quad (27)$$

188 Moreover, using (19) and the assumptions considered, then at the quadrature nodes one has  
189 for all  $k \in \{1, \dots, L\}$

$$\mathcal{P}_{\mathbf{S}}(-\theta_k^2) = -\frac{2 \sin(\pi\alpha) A \Gamma(1 + \alpha)}{\pi J_u} \mu_k \theta_k^{5-2\alpha} \prod_{\substack{j=1 \\ j \neq k}}^L (\theta_k^2 - \theta_j^2) \Rightarrow \text{sgn}(\mathcal{P}_{\mathbf{S}}(-\theta_k^2)) = (-1)^{L-k+1}.$$

190 Finally, the following limit holds

$$\mathcal{P}_{\mathbf{S}}(\lambda) \underset{\lambda \rightarrow -\infty}{\sim} (-1)^L \lambda^{L+2} \Rightarrow \text{sgn}(\mathcal{P}_{\mathbf{S}}(-\infty)) = 1. \quad (28)$$

191 We introduce the following intervals

$$\mathcal{I}_{L+1} = ]-\infty, -\theta_L^2], \quad \mathcal{I}_{\ell+1} = ]-\theta_{\ell+1}^2, -\theta_{\ell}^2] \quad \text{for } \ell = 1, \dots, L-1 \quad \text{and} \quad \mathcal{I}_1 = ]-\theta_1^2, 0]. \quad (29)$$

192 Given that  $\lambda \mapsto \mathcal{P}_{\mathbf{S}}(\lambda)$  is continuous, then equations (27–28) show that the polynomial  $\mathcal{P}_{\mathbf{S}}$   
193 changes sign in each of the intervals  $\mathcal{I}_{\ell}$  of (29). Consequently, there exist  $\lambda_{\ell} \in \mathcal{I}_{\ell}$  with  
194  $\ell = 1, \dots, L + 1$  such that  $\mathcal{P}_{\mathbf{S}}(\lambda_{\ell}) = 0$  and which coincide with the eigenvalues, with  
195 multiplicity 1, of the matrix  $\mathbf{S}$  of size  $L + 2$ .  $\square$

196 Proposition 3 states that, under suitable conditions on the quadrature coefficients, the  
197 matrix  $\mathbf{S}$  in (24) has eigenvalues with negative or zero real parts. This property is crucial  
198 regarding the numerical modeling developed in the forthcoming Section 4.2. As for the en-  
199 ergy analysis given in Proposition 1, positivity of quadrature nodes and weights is again the  
200 fundamental hypothesis. Lastly, it is possible to use the above proposition to characterize  
201 the spectral radius of the matrix  $\mathbf{S}$ .

202 **Proposition 4.** *The spectral radius of the matrix  $\mathbf{S}$  (24) is such that*

$$\max\left(\theta_L^2, (J_u\eta)^{-1} + \sum_{\ell=1}^L \mu_\ell \Upsilon_{\ell,\alpha}\right) \leq \varrho(\mathbf{S}) \leq \theta_L^2 + (J_u\eta)^{-1} + \sum_{\ell=1}^L \mu_\ell \Upsilon_{\ell,\alpha}.$$

203 *Proof.* By definition, one has

$$\text{tr}(\mathbf{S}) = -\left[(J_u\eta)^{-1} + \sum_{\ell=1}^L (\theta_\ell^2 + \mu_\ell \Upsilon_{\ell,\alpha})\right] \equiv \sum_{\ell=1}^{L+1} \lambda_\ell. \quad (30)$$

204 According to the proof of Property 3, the eigenvalues  $\lambda_\ell$  satisfy

$$-\sum_{\ell=1}^L \theta_\ell^2 \leq \sum_{\ell=1}^L \lambda_\ell \leq -\sum_{\ell=1}^{L-1} \theta_\ell^2.$$

205 Substitution in (30) and providing that  $\varrho(\mathbf{S}) = |\lambda_{L+1}|$  allows to concludes the proof.  $\square$

### 206 3.4. Semi-analytical solution

207 Let us consider a homogeneous Andrade–DA medium described by equations (20a)  
 208 and (20b), together with equation (15). A corresponding semi-analytical solution is sought  
 209 in order to validate the ensuing numerical simulations of wave propagation. It is assumed  
 210  $F_\sigma = 0$  and excitation  $F_v(x, t) = F(t)\delta(x - x_s)$  at source point  $x_s$  with time evolution  $F$ .  
 211 Applying space-time Fourier transforms and their inverses leads to the stress field solution  
 212 in the form of

$$\hat{\sigma}(x, \omega) = \frac{i\hat{F}(\omega)}{2\pi c_\infty^2 J_u} \int_{-\infty}^{+\infty} \frac{k}{k^2 - k_0^2} e^{ik(x-x_s)} \mathbf{d}k := \frac{i\hat{F}(\omega)}{2\pi c_\infty^2 J_u} \int_{-\infty}^{+\infty} g(k) \mathbf{d}k,$$

213 with

$$k_0 = \left[ \left(\frac{\omega}{c_\infty}\right)^2 \left[ 1 + \sum_{\ell=0}^L \frac{\mu_\ell \Upsilon_{\ell,\alpha}}{\theta_\ell^2 + i\omega} \right] - \frac{i\rho\omega}{\eta} \right]^{1/2}.$$

214 The poles  $\pm k_0$  of  $g$  are simple and satisfy  $\text{Im}[k_0] < 0$ . Using the residue theorem, one  
 215 obtains in the time-domain the stress field solution

$$\sigma(x, t) = -\frac{\text{sgn}(x - x_s)}{2\pi c_\infty^2 J_u} \int_0^{+\infty} \text{Re} \left[ \hat{F}(\omega) e^{i(\omega t - k_0|x-x_s|)} \right] \mathbf{d}\omega. \quad (31)$$

216 Similarly, the velocity field and the memory variables satisfy

$$\begin{aligned}
 v(x, t) &= \frac{1}{2\pi} \int_0^{+\infty} \operatorname{Re} \left[ \frac{k_0}{\omega} \hat{F}(\omega) e^{i(\omega t - k_0|x-x_s|)} \right] d\omega, \\
 \phi_\ell(x, t) &= -\frac{\operatorname{sgn}(x-x_s)\gamma_{\ell,\alpha}}{2\pi c_\infty^2} \int_0^{+\infty} \operatorname{Re} \left[ \frac{i\omega}{\theta_\ell^2 + i\omega} \hat{F}(\omega) e^{i(\omega t - k_0|x-x_s|)} \right] d\omega, \quad \ell = 1, \dots, L.
 \end{aligned}
 \tag{32}$$

217 In the numerical results presented Section 5, the frequency-domain integrals featured in  
 218 solutions (31) and (32) are computed using a standard quadrature rule over the frequency-  
 219 band considered.

## 220 4. Numerical methods

### 221 4.1. Quadrature methods

222 Two different approaches can be employed to determine the  $2L$  coefficients  $\{(\mu_\ell, \theta_\ell)\}_\ell$   
 223 of the diffusive approximation (16). While the most usual one is based on orthogonal  
 224 polynomials, the second approach is associated with an optimization procedure applied to  
 225 the model compliance. Both lead to positive quadrature coefficients, which ensures the  
 226 stability of the Andrade–DA model, as shown by propositions 1 and 3.

227 *Gaussian quadrature.* Various orthogonal polynomials can be used to evaluate the im-  
 228 proper integral (13) introduced by the diffusive representation of fractional derivatives.  
 229 Historically, the first one has been proposed in [22], where a Gauss-Laguerre quadrature  
 230 is chosen. Its slow convergence was highlighted and then corrected in [23] with a Gauss-  
 231 Jacobi quadrature. This latter method has been lastly modified in [24], where alterna-  
 232 tive weight functions are introduced, yielding an improved discretization of the diffusive  
 233 variable owing to the use of an extended interpolation range. Following this latter modi-  
 234 fied Gauss-Jacobi approach, while omitting the time and space coordinates for the sake of  
 235 brevity, the improper integral (13) is then recast as

$$\int_0^{+\infty} \phi(\theta) d\theta = \int_{-1}^{+1} (1-\tilde{\theta})^\gamma (1+\tilde{\theta})^\delta \tilde{\phi}(\tilde{\theta}) d\tilde{\theta} \simeq \sum_{\ell=1}^L \tilde{\mu}_\ell \tilde{\phi}(\tilde{\theta}_\ell), \tag{33}$$

236 with the modified diffusive variable  $\tilde{\phi}$  defined as

$$\tilde{\phi}(\tilde{\theta}) = \frac{4}{(1 - \tilde{\theta})^{\gamma-1} (1 + \tilde{\theta})^{\delta+3}} \phi\left(\left(\frac{1 - \tilde{\theta}}{1 + \tilde{\theta}}\right)^2\right),$$

237 and where the weights and nodes  $\{(\tilde{\mu}_\ell, \tilde{\theta}_\ell)\}_\ell$  can be computed by standard routines [32].

238 According to the analysis of [24], Section 4, an optimal choice for the coefficients in (33)

239 is in the present case:  $\gamma = 3 - 4\alpha$  and  $\delta = 4\alpha - 1$ . Finally, the quadrature coefficients of

240 (16) are identified as

$$\mu_\ell = \frac{4 \tilde{\mu}_\ell}{(1 - \tilde{\theta}_\ell)^{\gamma-1} (1 + \tilde{\theta}_\ell)^{\delta+3}}, \quad \theta_\ell = \left(\frac{1 - \tilde{\theta}_\ell}{1 + \tilde{\theta}_\ell}\right)^2. \quad (34)$$

241 *Optimization quadrature..* Alternatively, the quadrature coefficients can be deduced from

242 the model physical observables. Note that as the quality factor (11) is defined as the ratio

243  $Q(\omega) = -\text{Re}[N]/\text{Im}[N]$ , then optimizing an objective function based on the latter would

244 entail an indetermination on the function  $N$ , i.e. of the model constitutive equation. There-

245 fore, a direct optimization of the available Andrade model compliance  $N$  is preferred.

246 From (5) and its diffusive approximated counterpart (17), the corresponding compli-

247 ances  $N$  and  $\tilde{N}$  differ only in the terms

$$\begin{cases} \kappa(\omega) := (i\omega)^{-\alpha} & \text{Andrade,} \\ \tilde{\kappa}(\omega) := \frac{2 \sin(\pi\alpha)}{\pi} \sum_{\ell=1}^L \mu_\ell \frac{\theta_\ell^{1-2\alpha}}{\theta_\ell^2 + i\omega} & \text{Andrade-DA.} \end{cases}$$

248 For a given number  $K$  of angular frequencies  $\omega_k$ , one introduces the objective function

$$\mathcal{J}\left(\{(\mu_\ell, \theta_\ell)\}_\ell; L, K\right) = \sum_{k=1}^K \left| \frac{\tilde{\kappa}(\omega_k)}{\kappa(\omega_k)} - 1 \right|^2 = \sum_{k=1}^K \left| \frac{2 \sin(\pi\alpha)}{\pi} \sum_{\ell=1}^L \mu_\ell \frac{\theta_\ell^{1-2\alpha} (i\omega_k)^\alpha}{\theta_\ell^2 + i\omega_k} - 1 \right|^2 \quad (35)$$

249 to be minimized w.r.t parameters  $\{(\mu_\ell, \theta_\ell)\}_\ell$  for  $\ell = 1, \dots, L$ .

250 A straightforward linear minimization of (35) may lead to some negative parameters

251 [33, 34] so that a nonlinear optimization with the positivity constraints  $\mu_\ell \geq 0$  and  $\theta_\ell \geq 0$

252 is preferred. The additional constraint  $\theta_\ell \leq \theta_{\max}$  is also introduced to avoid the algorithm



253 to diverge. These  $3L$  constraints can be relaxed by setting  $\mu_\ell = \mu_\ell'^2$  and  $\theta_\ell = \theta_\ell'^2$  and  
 254 solving the following problem with only  $L$  constraints

$$\min_{\{(\theta_\ell', \mu_\ell')\}_\ell} \mathcal{J}\left(\{(\mu_\ell'^2, \theta_\ell'^2)\}_\ell; L, K\right) \quad \text{with } \theta_\ell'^2 \leq \theta_{\max} \text{ for } \ell = 1, \dots, L. \quad (36)$$

255 As problem (36) is nonlinear and non-quadratic w.r.t. abscissae  $\theta_\ell'$ , we implement the  
 256 algorithm SolvOpt [35, 36] based on the iterative Shor's method [37]. Initial values  $\mu_\ell'^0$   
 257 and  $\theta_\ell'^0$  used in the algorithm must be chosen with care; for this purpose we propose to use  
 258 the coefficients obtained by the modified Jacobi method (34) for  $\ell = 1, \dots, L$

$$\mu_\ell'^0 = \sqrt{\frac{4\tilde{\mu}_\ell}{(1 - \tilde{\theta}_\ell)^{\gamma-1}(1 + \tilde{\theta}_\ell)^{\delta+3}}}, \quad \theta_\ell'^0 = \frac{1 - \tilde{\theta}_\ell}{1 + \tilde{\theta}_\ell}. \quad (37)$$

259 Finally, the angular frequencies  $\omega_k$  for  $k = 1, \dots, K$  in (35) are chosen linearly on a loga-  
 260 rithmic scale over a given optimization band  $[\omega_{\min}, \omega_{\max}]$ , i.e.

$$\omega_k = \omega_{\min} \left( \frac{\omega_{\max}}{\omega_{\min}} \right)^{\frac{k-1}{K-1}}. \quad (38)$$

261 **Remark 1.** In the proposed optimization method, both set of quadrature coefficients  $\mu_\ell$   
 262 and  $\theta_\ell$  are computed by minimization of the objective function  $\mathcal{J}$ . In particular, the nodes  
 263  $\theta_\ell$  are not imposed to be equidistributed according to (38) as it is the case in the commonly  
 264 used approach [13]. This point will be returned to in Section 5.2.

#### 265 4.2. Numerical scheme

266 A numerical scheme is proposed to compute the solution of system (22). Introducing a  
 267 uniform grid with mesh size  $\Delta x$  and time step  $\Delta t$ , let  $\mathbf{U}_j^n$  denotes the approximation of the  
 268 solution  $\mathbf{U}(x_j = j\Delta x, t_n = n\Delta t)$  with  $j = 1, \dots, N_x$  and  $n = 1, \dots, N_t$ . Straightforward  
 269 discretization of (22) typically yields to the numerical stability condition [33]

$$\Delta t \leq \min \left( \frac{\Delta x}{c_\infty}, \frac{2}{\varrho(\mathbf{S})} \right).$$

270 As shown by Proposition 4, the usual CFL bound on the time step  $\Delta t \leq \Delta x/c_\infty$  may be  
 271 reduced as  $\eta$  decreases or  $A$  increases, which turns out to be detrimental to the numerical

272 scheme. Moreover, as  $\varrho(\mathbf{S})$  depends on the quadrature coefficients of the diffusive variable  
 273 the stability condition would in turn not depend only on meaningful physical quantities  
 274 such as the maximum phase velocity  $c_\infty$ .

275 *Splitting..* Alternatively, we follow here the splitting approach analyzed in [29]. To imple-  
 276 ment (22) numerically, one solves successively the propagative equation

$$\frac{\partial \mathbf{U}}{\partial t} + \mathbf{A} \frac{\partial \mathbf{U}}{\partial x} = \mathbf{0} \quad (39)$$

277 and the diffusive equation

$$\frac{\partial \mathbf{U}}{\partial t} = \mathbf{S} \mathbf{U} + \mathbf{F}. \quad (40)$$

278 Due to the structure of matrix  $\mathbf{S}$ , one defines from (21) the subvectors

$$\bar{\mathbf{U}} = [\sigma, \phi_1, \dots, \phi_L]^\top, \quad \bar{\mathbf{F}} = [F_\sigma, J_u \gamma_{1,\alpha} F_\sigma, \dots, J_u \gamma_{L,\alpha} F_\sigma]^\top, \quad (41)$$

279 and from (24) the submatrix

$$\bar{\mathbf{S}} = \begin{bmatrix} -(J_u \eta)^{-1} & -A\Gamma(1 + \alpha)J_u^{-1}\mu_1 & \cdots & -A\Gamma(1 + \alpha)J_u^{-1}\mu_L \\ -\gamma_{1,\alpha}\eta^{-1} & -\theta_1^2 - \Upsilon_{1,\alpha}\mu_1 & \cdots & -\Upsilon_{1,\alpha}\mu_L \\ \vdots & \vdots & \ddots & \vdots \\ -\gamma_{L,\alpha}\eta^{-1} & -\Upsilon_{L,\alpha}\mu_1 & \cdots & -\theta_L^2 - \Upsilon_{L,\alpha}\mu_L \end{bmatrix}.$$

Having separated the two source terms, then equation (40) is equivalently recast in the form

$$\begin{cases} \frac{\partial v}{\partial t} = F_v, & (42a) \\ \frac{\partial \bar{\mathbf{U}}}{\partial t} = \bar{\mathbf{S}} \bar{\mathbf{U}} + \bar{\mathbf{F}}. & (42b) \end{cases}$$

280 The discrete operators associated with the discretizations of (39) and (42) are respec-  
 281 tively denoted by  $\mathcal{H}_p$  and  $\mathcal{H}_d$ . The operator  $\mathcal{H}_d$  depends explicitly on time when the  
 282 forcing terms  $F_v$  or  $F_\sigma$  are non-zero, whereas  $\mathcal{H}_p$  remains independent on  $t$ . The so-  
 283 called Strang splitting approach of [29] is then used between time steps  $t_n$  and  $t_{n+1}$ , for

284  $n = 0, \dots, N_t - 1$ , which requires to solve (39) and (40) with adequate time increments  
 285 as, for  $j = 1, \dots, N_x$

$$\begin{aligned} \mathbf{U}_j^{(1)} &= \mathcal{H}_d(t_n, \Delta t/2) \mathbf{U}_j^n, \\ \mathbf{U}_j^{(2)} &= \mathcal{H}_p(\Delta t, j) \mathbf{U}^{(1)}, \\ \mathbf{U}_j^{n+1} &= \mathcal{H}_d(t_{n+1}, \Delta t/2) \mathbf{U}_j^{(2)}, \end{aligned} \quad (43)$$

286 with  $\mathbf{U}^{(1)} = [\mathbf{U}_1^{(1)} \dots \mathbf{U}_{N_x}^{(1)}]^\top$ . Since the matrices  $\mathbf{A}$  and  $\mathbf{S}$  do not commute, an error  
 287 associated with the splitting scheme is introduced [29]. However, provided that  $\mathcal{H}_p$  and  
 288  $\mathcal{H}_d$  are at least second-order accurate and stable, then the time-marching scheme (43)  
 289 constitutes a second-order accurate approximation of the original equation (22).

290 **Diffusive operator.** The physical parameters do not vary with time, thus the matrix  
 291  $\bar{\mathbf{S}}$  does not depend on  $t$ . Owing to Property 3, one has  $0 \notin \text{sp}(\bar{\mathbf{S}}) = \{\lambda_1, \dots, \lambda_L\}$ , and  
 292 hence  $\det \bar{\mathbf{S}} \neq 0$ . Freezing the forcing terms at  $t_k$ , with  $k = n$  or  $n + 1$ , yields for a generic  
 293 vector  $\mathbf{U}_j = [v_j, \bar{\mathbf{U}}_j]^\top$

$$\mathcal{H}_d(t_k, \Delta t/2) \mathbf{U}_j = \left[ v_j + \frac{\Delta t}{2} F_v(x_j, t_k), e^{\bar{\mathbf{S}} \frac{\Delta t}{2}} \bar{\mathbf{U}}_j - \left( \mathbf{I} - e^{\bar{\mathbf{S}} \frac{\Delta t}{2}} \right) \bar{\mathbf{S}}^{-1} \bar{\mathbf{F}}(x_j, t_k) \right]^\top. \quad (44)$$

294 If there is no excitation, i.e.  $F_v = F_\sigma = 0$ , then integration (44) is exact. The matrix  
 295 exponential entering the definition of the operator  $\mathcal{H}_d$  is computed using the method #2 in  
 296 [38] based on a (6/6) Padé approximation. Property 3 ensures that the computation of this  
 297 exponential is stable.

298 **Propagative operator.** To integrate (39), we use a fourth-order ADER (Arbitrary  
 299 DERivative) scheme [39]. This explicit two-step and single-grid finite-difference scheme  
 300 writes

$$\mathbf{U}_j^{(2)} = \mathbf{U}_j^{(1)} - \sum_{\ell=-2}^{\ell=2} \sum_{m=1}^4 \vartheta_{m,\ell} \left( \mathbf{A} \frac{\Delta t}{\Delta x} \right)^m \mathbf{U}_{j+\ell}^{(1)} := \mathcal{H}_p(\Delta t, j) \mathbf{U}^{(1)}, \quad (45)$$

301 where the coefficients  $\vartheta_{m,k}$  are provided in Table 1. It satisfies the optimal stability condi-  
 302 tion  $c_\infty \Delta t / \Delta x \leq 1$ .

	$m = 1$	$m = 2$	$m = 3$	$m = 4$
$\ell = -2$	1/12	1/24	-1/12	-1/24
$\ell = -1$	-2/3	-2/3	1/6	1/6
$\ell = 0$	0	5/4	0	1/4
$\ell = 1$	2/3	-2/3	-1/6	1/6
$\ell = 2$	-1/12	1/24	1/12	-1/24

Table 1: Coefficients  $\vartheta_{m,\ell}$  in the ADER-4 scheme (45)

## 303 5. Numerical results

### 304 5.1. Configuration

305 The homogeneous domain considered is 400 m-long and it is characterized by the phys-  
306 ical parameters provided in Table 2 and which are consistent with experimentally-based  
307 values, see [19] and the references therein.

$\rho$ (kg/m <sup>3</sup> )	$c_\infty$ (m/s)	$\eta$ (Pa.s)	$A$ (Pa <sup>-1</sup> .s <sup>-<math>\alpha</math></sup> )	$\alpha$
1200	2800	10 <sup>9</sup>	2 10 <sup>-10</sup>	1/3

Table 2: Chosen physical parameters in the Andrade model (4).

### 308 5.2. Validation of the quadrature methods

309 The angular frequency range of interest  $[\omega_{\min}, \omega_{\max}]$  is defined by  $\omega_{\min} = \omega_c/100$  and  
310  $\omega_{\max} = 10 \omega_c$  for a given central angular frequency  $\omega_c = 60 \pi$ , while we set  $\theta_{\max} = \sqrt{100 \omega_c}$   
311 and  $K = 2 L$ . Observables of the original Andrade model (5) are then compared to those  
312 of the Andrade-DA model (17) on Figure 2 for the two quadrature methods discussed  
313 in Section 4.1. Large deviations are observed when the Gaussian quadrature is used, in  
314 particular on the attenuation function. On the contrary, an excellent agreement between the  
315 original Andrade model and its diffusive counterpart is obtained. Only slight differences  
316 can be observed at the scale of the figures within the optimization interval.

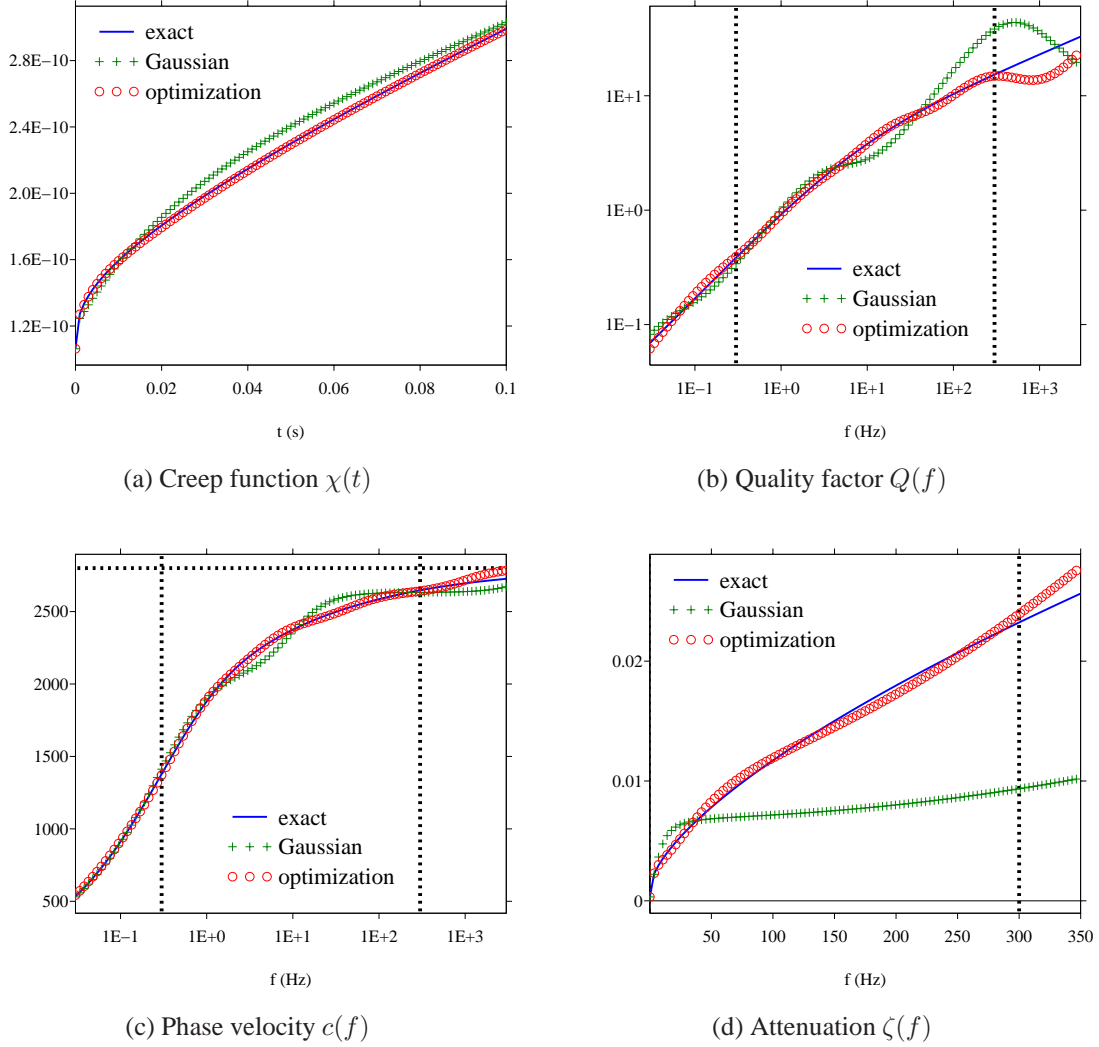


Figure 2: Comparison between exact observables of the Andrade model and their approximate counterparts, for  $L = 4$  memory variables. The physical parameters are given in Table 2. Vertical dotted lines delimit the optimization frequency-band. The horizontal dotted line in panel (c) denotes the high-frequency limit  $c_\infty$ .

317 On Figure 3 are represented the  $L = 4$  and  $L = 8$  quadrature coefficients, i.e. nodes  
 318  $\theta_\ell$  with corresponding weights  $\mu_\ell$ , for the two methods considered. Note that, according to  
 319 (37), the values provided by the Gaussian approach are used as initial guesses in the mini-  
 320 mization (36). The scaled optimization angular frequencies  $\sqrt{\omega_k}$  for  $k = 1, \dots, K$  are also

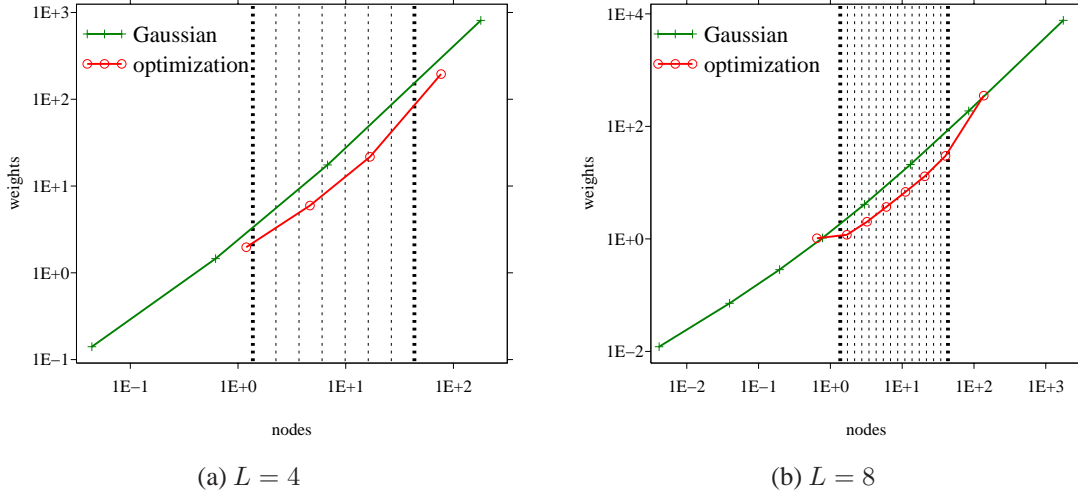


Figure 3: Quadrature coefficients  $\{(\mu_\ell, \theta_\ell)\}_\ell$  for the two approaches considered. Vertical dotted lines denote the  $K = 2L$  scaled optimization angular frequencies  $\sqrt{\omega_k}$ .

321 shown for the purposes of comparison. Remarkably, the computed optimal nodes do not  
 322 coincide with equidistributed nodes along the optimization frequency-band, a repartition  
 323 which is prescribed in the commonly employed approach of [13].

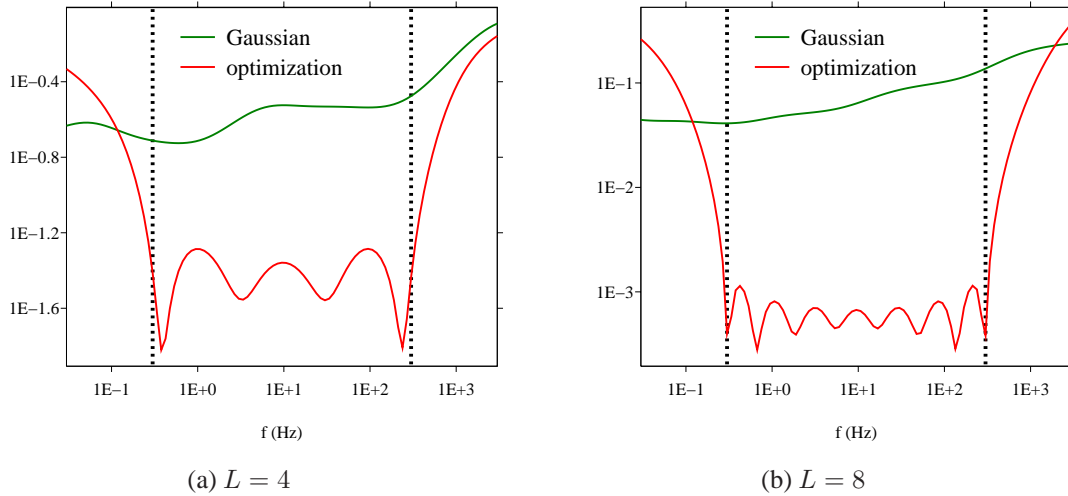


Figure 4: Computed error  $|\frac{\tilde{\kappa}(f)}{\kappa(f)} - 1|$ . Vertical dotted lines delimit the optimization frequency-band.

324 The corresponding model error defined as  $|\frac{\tilde{\kappa}(\omega)}{\kappa(\omega)} - 1|$  and associated with the minimiza-  
 325 tion problem (36) is displayed in Figure 4, for  $L = 4$  (Fig. 4a) and  $L = 8$  (Fig. 4b) diffusive  
 326 variables. For a given quadrature method, the results are clearly improved as  $L$  increases.  
 327 For a given  $L$ , the optimization provides more accurate results compared to the Gaussian  
 328 quadrature over the frequency band of interest which is delimited by vertical dotted lines.

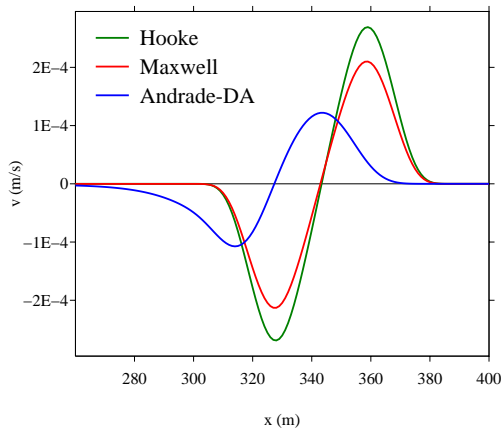
### 329 5.3. Validation of the numerical scheme

330 While  $F_\sigma = 0$  in (20b), the source in (20a) is imposed at point  $x_s$  as  $F_v(x, t) =$   
 331  $F(t) \delta(x - x_s)$  where  $F(t)$  is the  $C^6$  function

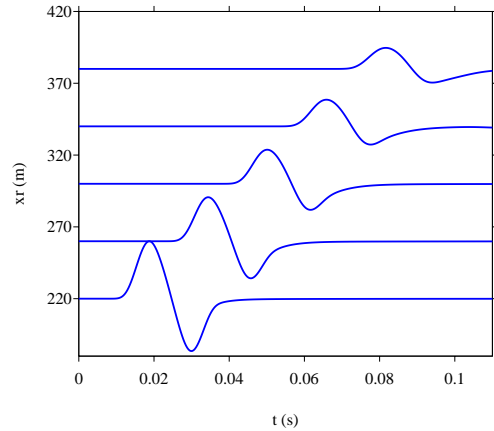
$$332 F(t) = \begin{cases} \sin(\omega_c t) - \frac{21}{32} \sin(2\omega_c t) + \frac{63}{768} \sin(4\omega_c t) - \frac{1}{512} \sin(8\omega_c t) & \text{if } 0 \leq t \leq \frac{1}{f_c}, \\ 0 & \text{otherwise} \end{cases} \quad (46)$$

332 with the central frequency  $f_c = \omega_c/2\pi = 30$  Hz. Moreover, the domain is discretized with  
 333  $N_x = 400$  nodes and the diffusive approximation is computed by constrained optimization  
 334 with  $L = 4$  memory variables and thus  $K = 8$  optimization frequencies. The CFL condi-  
 335 tion is chosen so that  $c_\infty \Delta t / \Delta x = 0.95$  and the time integration is performed up to final  
 336 time  $t_f = 200\Delta t \approx 67$  ms based on the fourth order ADER scheme, see Sec. 4.2. Fol-  
 337 lowing Section 3.4, the semi-analytical solution of the Andrade–DA model is computed by  
 338 discrete inverse Fourier transform on 2048 modes, with uniform frequency step  $\Delta f = 0.15$   
 339 Hz. The solution is recorded at each time step at receivers located at  $x_r = 220 + 40(r - 1)$   
 340 for  $r = 1, \dots, 5$ .

341 Figure 5 displays snapshots of forward propagating waves from the source point  $x_s =$   
 342 200. The numerical solutions associated with various values of the attenuation parameters  
 343 in (18) are plotted on Fig. 5a; namely Hooke model (i.e. purely elastic case which may  
 344 be obtained in the limit  $\eta = +\infty$  and setting  $A = 0$ ), Maxwell model ( $A = 0, \eta =$   
 345  $10^9$ ), and Andrade–DA model ( $A = 2 \cdot 10^{-9}, \eta = 10^9$ ). As predicted by the dispersion  
 346 analysis of sections 2.3 and 2.4, the phase velocity of the Andrade–DA model, as this of its  
 347 original version, is lower than in the elastic case, which explains the observed delay. Figure



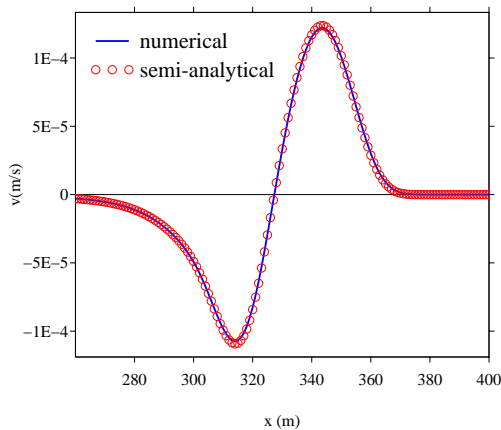
(a) Snapshots at  $t_f$



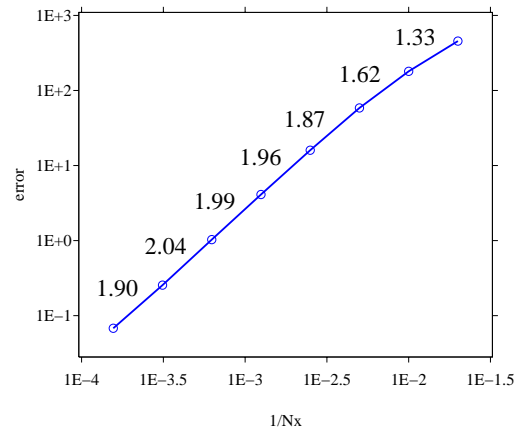
(b) Time evolution for the Andrade-DA model

Figure 5: Time-domain numerical simulations of wave propagation.

348 **5b** shows a seismogram corresponding to the Andrade-DA model in order to highlight  
 349 attenuation and dispersion of the waveform.



(a) Semi-analytical and numerical solutions



(b) Convergence measurements with numbers indicating slopes between two neighboring points

Figure 6: Validation of the numerical scheme for the Andrade-DA model.

350 Figure 6 compares the semi-analytical and numerical solutions of Andrade-DA model  
 351 corresponding to equations (32) and (20), respectively. Figure 6b presents convergence  
 352 measurements done for various discretizations, varying the numbers of nodes in the interval



353  $N_x = 50$  to 6400. Order 2 is reached, confirming the theoretical results of Section 4.2.

## 354 **6. Conclusion**

355 Wave propagation phenomena associated with a fractional viscoelastic medium are in-  
356 vestigated in this study. The Andrade model is used as a prototypical reference constitu-  
357 tive equation as it satisfactorily describes the transient behaviors of metals and geological  
358 media. A diffusive representation of the featured non-local fractional derivative term is  
359 introduced to convert the associated convolution product into an integral of a function sat-  
360 isfying a local ordinary differential equation. Based on a quadrature approximation of this  
361 integrated term, a system of local partial differential equations is finally obtained and is  
362 shown to be well-suited for a numerical implementation.

363 The system at hand is investigated and it is demonstrated that its well-posedness re-  
364 quires the positiveness of the weights associated with the quadrature scheme. To compute  
365 the quadrature coefficients, two numerical methods are combined: a polynomial Gaussian  
366 approach to get an initial guess jointly with a constrained optimization to approximate  
367 the Andrade model compliance over a frequency-band of interest. It is shown that the  
368 properties of the original Andrade model are well approximated by those of the computed  
369 Andrade–DA model. Finally, an explicit time-domain finite-difference scheme is described  
370 and implemented. Corresponding wave propagation numerical experiments are presented  
371 and the efficiency of the proposed approach is highlighted. The main point of this arti-  
372 cle is that using a diffusive approximation of a fractional derivative term, entering a given  
373 viscoelastic constitutive equation, yields a sound mathematical model, that is also easily  
374 tractable numerically to perform wave propagation simulations.

375 To focus on this message, a simple but realistic fractionally-damped viscoelastic model  
376 within a unidimensional and homogeneous configuration has been considered. Its dynami-  
377 cal behavior is described by a first-order hyperbolic system which extension to higher spa-  
378 tial dimensions or heterogeneous media is straightforward. Moreover, efficient numerical  
379 methods are currently available and can be directly employed to perform corresponding

380 time-domain simulations. Alternatively, arbitrary-shaped material discontinuities within  
381 piecewise-homogeneous 2D Andrade media can be handled using an immersed interface  
382 method [40]. Work is currently done on the subject.

383 Another line of research concerns extension of the proposed approach to other frac-  
384 tional viscoelastic model, such as the fractional Kelvin-Voigt model [41, 28] or the frac-  
385 tional Zener model [42, 43]. More sophisticated models could also be investigated, such  
386 as nonlinear fractional viscoelasticity [44] or nonlocal models in space [45].

387 *Acknowledgements.* The work of Abderrahmin Ben Jazia has been funded by the Ecole  
388 Centrale de Marseille, France, for which special thanks are addressed to Guillaume Chi-  
389 avassa. The authors are thankful to Emilie Blanc for fruitful discussions

## 390 **References**

- 391 [1] E. N. d. C. Andrade, On the viscous flow in metals, and allied phenomena, Proc. Roy.  
392 Soc. A 84 (567) (1910) 1–12.
- 393 [2] T. L. Szabo, Time domain wave equations for lossy media obeying a frequency power  
394 law, J. Acoust. Soc. Am. 96 (1994) 491–500.
- 395 [3] T. L. Szabo, Causal theories and data for acoustic attenuation obeying a frequency  
396 power law, J. Acoust. Soc. Am. 97 (1995) 14–24.
- 397 [4] M. P. Flanagan, D. Wiens, Attenuation of broadband P and S waves in Tonga: Obser-  
398 vations of frequency dependent Q, P. App. Geophys. 153 (1998) 345–375.
- 399 [5] V. Lekić, J. Matas, M. Panning, B. Romanowicz, Measurement and implications of  
400 frequency dependence of attenuation, Earth And Planetary Science Letters 282 (2009)  
401 285–293.
- 402 [6] P. J. Torvik, R. L. Bagley, On the appearance of the fractional derivative in the behav-  
403 ior of real materials, J. Appl. Mech. 51 (1985) 294–298.

- 404 [7] J. M. Carcione, Wave Fields in Real Media: Wave propagation in Anisotropic,  
405 Anelastic and Porous Media, Pergamon, 2001.
- 406 [8] I. Podlubny, Fractional Differential Equations, Academic Press, 1999.
- 407 [9] F. Mainardi, Fractional Calculus and Waves in Linear Viscoelasticity. An Introduction  
408 to Mathematical Models, Imperial College Press, 2010.
- 409 [10] S. Holm, S. P. Näsholm, A causal and fractional all-frequency wave equation for lossy  
410 media, J. Acous. Soc. Am. 130 (4) (2011) 2195–2202.
- 411 [11] K. R. Waters, J. Mobley, J. G. Miller, Causality-imposed (Kramers-Kronig) relation-  
412 ships between attenuation and dispersion, IEEE Trans. Ultrason. Ferroelectr. Freq.  
413 Control. 52 (2005) 822–33.
- 414 [12] K. R. Waters, M. S. Hughes, J. Mobley, G. H. Brandenburger, J. G. Miller, On the ap-  
415 plicability of Kramers-Krönig relations for ultrasonic attenuation obeying a frequency  
416 power law, J. Acoust. Soc. Am. 108 (2000) 556–563.
- 417 [13] H. Emmerich, M. Korn, Incorporation of attenuation into time-domain computations  
418 of seismic wave fields, Geophysics 52 (1987) 1252–1264.
- 419 [14] S. P. Näsholm, S. Holm, Linking multiple relaxation, power-law attenuation, and  
420 fractional wave equations, J. Acous. Soc. Am. 130 (5) (2011) 3038–3045.
- 421 [15] E. N. d. Andrade, On the validity of  $t^{1/3}$  law of flow of metals, Philos. Mag. 7 (84)  
422 (1962) 2003–2014.
- 423 [16] T. T. Gribb, R. F. Cooper, Low-frequency shear attenuation in polycrystalline olivine:  
424 Grain boundary diffusion and the physical significance of the Andrade model for  
425 viscoelastic rheology, J. Geophys. Res. Solid Earth 103 (B11) (1998) 27267–27279.

- 426 [17] I. Jackson, U. H. Faul, Grainsize-sensitive viscoelastic relaxation in olivine: Towards  
427 a robust laboratory-based model for seismological application, *Physics of the Earth  
428 and Planetary Interiors* 183 (1-2) (2010) 151–163.
- 429 [18] M. Sundberg, R. F. Cooper, A composite viscoelastic model for incorporating grain  
430 boundary sliding and transient diffusion creep: Correlating creep and attenuation re-  
431 sponses for materials with a fine grain size, *Philos. Mag.* 90 (20) (2010) 2817–2840.
- 432 [19] C. Bellis, B. Holtzman, Sensitivity of seismic measurements to frequency-dependent  
433 attenuation and upper mantle structure: an initial approach, submitted (2013).
- 434 [20] A. C. Galucio, J.-F. Deü, R. Ohayon, Finite element formulation of viscoelastic sand-  
435 wich beams using fractional derivative operators, *Comput. Mech.* 33 (4) (2004) 282–  
436 291.
- 437 [21] D. Matignon, Stability properties for generalized fractional differential systems,  
438 *ESAIM: Proc.* 5 (1998) 145–158.
- 439 [22] L. Yuan, O. P. Agrawal, A numerical scheme for dynamic systems containing frac-  
440 tional derivatives, *J. Vib. Acoust.* 124 (2002) 321–324.
- 441 [23] K. Diethelm, An investigation of some nonclassical methods for the numerical ap-  
442 proximation of Caputo-type fractional derivatives, *Numer. Algor.* 47 (2008) 361–390.
- 443 [24] C. Birk, C. Song, An improved non-classical method for the solution of fractional  
444 differential equations, *Comput. Mech.* 46 (2010) 721–734.
- 445 [25] H. Haddar, J.-R. Li, D. Matignon, Efficient solution of a wave equation with  
446 fractional-order dissipative terms, *J. Comput. Appl. Math.* 234 (2010) 2003–2010.
- 447 [26] J.-F. Deü, D. Matignon, Simulation of fractionally damped mechanical systems by  
448 means of a Newmark-diffusive scheme, *Comput. Math. Appl.* 59 (2010) 1745–1753.

- 449 [27] M. G. Wismer, Finite element analysis of broadband acoustic pulses through inho-  
450 mogenous media with power law attenuation, *J. Acous. Soc. Am.* 120 (2006) 3493–  
451 3502.
- 452 [28] M. Caputo, J. M. Carcione, F. Cavallini, Wave simulation in biologic media based  
453 on the Kelvin-Voigt fractional-derivative stress-strain relation, *Ultrasound Med. Biol.*  
454 37 (6) (2011) 996–1004.
- 455 [29] R. J. LeVeque, *Numerical Methods for Conservation Laws*, 2nd Edition, Birkhäuser-  
456 Verlag, 1992.
- 457 [30] A. Hanyga, On wave propagation in viscoelastic media with concave creep compli-  
458 ance, arXiv:1302.1797v2 (2013).
- 459 [31] A. Hanyga, Wave propagation in linear viscoelastic media with completely monotonic  
460 relaxation moduli, arXiv:1302.0402v2 (2013).
- 461 [32] B. Flannery, W. Press, S. Teukolsky, W. Vetterling, *Numerical Recipes in C: the Art*  
462 *of Scientific Computing*, Cambridge University Press, 1992.
- 463 [33] E. Blanc, Numerical modeling of transient poroelastic waves: the Biot-JKD model  
464 with fractional derivatives, Ph.D. thesis, Aix-Marseille Université (2013).
- 465 [34] E. Blanc, G. Chiavassa, B. Lombard, Biot-JKD model: simulation of 1D transient  
466 poroelastic waves with fractional derivatives, *J. Comput. Phys.* 237 (2013) 1–20.
- 467 [35] F. Kappel, A. Kuntsevich, An implementation of Shor’s r-algorithm, *Comput. Optim.*  
468 *Appl.* 15 (2) (2000) 193–205.
- 469 [36] A. Rekik, R. Brenner, Optimization of the collocation inversion method for the linear  
470 viscoelastic homogenization, *Mech. Res. Com.* 38 (2011) 305–308.
- 471 [37] N. Shor, *Minimization Methods for Non-Differentiable Functions*, Springer-Verlag,  
472 1985.

- 473 [38] C. Moler, C. Van Loan, Nineteen dubious ways to compute the exponential of a ma-  
474 trix, twenty-five years later, *SIAM Review* 45 (2003) 3–49.
- 475 [39] T. Schwartzkopff, M. Dumbser, C. Munz, Fast high-order order schemes for linear  
476 hyperbolic equations, *J. Comput. Phys.* 197 (2) (2004) 532–539.
- 477 [40] G. Chiavassa, B. Lombard, Time domain numerical modeling of wave propagation in  
478 2D heterogeneous porous media, *J. Comput. Phys.* 230 (2011) 5288–5309.
- 479 [41] M. Caputo, Linear models of dissipation whose  $Q$  is almost frequency independent,  
480 part II, *Geophys. J. R. Astr. Soc.* 13 (1967) 529–539.
- 481 [42] T. Pritz, Analysis of four-parameter fractional derivative model of real solid materials,  
482 *J. Sound Vib.* 100 (1996) 1301–1315.
- 483 [43] S. P. Näsholm, S. Holm, On a fractional Zener elastic wave equation, *Fract. Calc.*  
484 *Appl. Anal.* 16 (2013) 26–50.
- 485 [44] A. Hanyga, Fractional-order relaxation laws in non-linear viscoelasticity, *Continuum*  
486 *Mech. Thermodyn.* 19 (2007) 25–36.
- 487 [45] A. Hanyga, M. Seredynska, Spatially fractional-order viscoelasticity, non-locality,  
488 and a new kind of anisotropy, *J. Math. Phys.* 53 (2012) 052902.